Dynamic Wetting of Photo-Responsive Arylazopyrazole Monolayers is Controlled by the Molecular Kinetics of the Monolayer

Christian Honnigfort[1,2], Leon Topp[1], Natalia García Rey[1], Andreas Heuer[1], and Björn Braunschweig[1,2],*

1) Institute of Physical Chemistry, Westfälische Wilhelms-Universität Münster, Corrensstraße 28/30, 48149 Münster, Germany

2) Center of Soft Nanoscience, Westfälische Wilhelms-Universität Münster, Busso-Peus-Straße 10, 48149 Münster, Germany

Corresponding Author *e-mail: braunschweig@uni-muenster.de.

ABSTRACT

Smart surfaces that can change their wettability on demand are interesting for applications such as self-cleaning surfaces or lab-on-a-chip devices. We have synthesized arylazopyrazole phosphonic acids (AAP) as a new class of photoswitchable molecules for functionalization of aluminum oxide surfaces. AAP monolayers were deposited on α-Al$_2$O$_3$(0001) and showed reversible E/Z photo-switching that can trigger contact angle changes of up to ~10°. We monitored these changes on the macroscopic level by recording the contact angle while the monolayer was switched *in situ*. On the molecular level, time-dependent vibrational sum-frequency generation (SFG) spectroscopy provided information on the kinetic changes within the AAP monolayer and the characteristic times for E/Z switching. In addition, vibrational SFG at different relative humidity indicates that the thermal stability of the Z configuration is largely influenced by the presence of water which can stabilize the Z state and hinder E$\rightarrow$Z switching of the AAP monolayer when it is wetted with H$_2$O. Having established the switching times on the

molecular scale, we additionally measured the dynamic contact angle and show that the time scales of the substrate and droplet dynamics can be extracted individually. For that, we report on a relaxation model, that is solved analytically and is verified via a comparison with simulations of a Lennard Jones system and with experimental data. The slower E to Z switching in the presence of the droplet as compared to the vapor phase is rationalized in terms of specific interactions of water with the exposed AAP moieties.

INTRODUCTION

Changing the wetting properties of surfaces dynamically and reversibly is of great interest for applications such as self-cleaning surfaces,[1] microfluidics[2] or lab-on-a-chip devices, just to mention a few.[3] However, a quantitative description and experiments are challenging when the wetting dynamics are dominated by the adaptation of a flexible substrate to a wetting liquid or by the photo-induced switching of the solids wettability.[4–6] Here, in particular the relevant time scales need to be addressed on the molecular level of the interfacial region that causes the wettability change. However, this is often challenging as in many systems the wettability change is dominated by the non-equilibrium properties of a single molecular layer which are often not accessible in experiments.

For that reason, wetting of molecular photoswitches such as azobenzene derivatives, diarylethenes[7] or spiropyranes[8] has been addressed mostly under equilibrium conditions. Detailed information on wetting dynamics of photoswitchable surfaces as well as on the associated molecular structure changes of photo-switchable molecular monolayers is, in fact, scarce.[9–12] Arylazopyrazoles (AAP) have been recently introduced as a new class of photo-switchable molecules that exhibit advantages over existing systems.[13–16] Similar to azobenzenes,[9,12,17–19] AAPs can change their E/Z configuration by photoisomerization using 520 nm visible or 365 nm UV light,[20–22] but are considered as superior analogues to azobenzene derivatives because of their high photostationary states of >90% for switching in both directions and their remarkably long thermal half-life times.[18,23,24]

Depending on the system under investigation, the light-induced changes of the contact angle Θ vary to a large extend. For instance, Kwon et al.[25] showed for dye-sensitized TiO_2 surfaces that Θ was changed reversibly by ~40° when the samples were irradiated with light. This is largely different for

nanoscopically flat thin films of polymers having an azobenzene group and fluorinated residues. Groten et al.[26] demonstrated that the light-induced changes in Θ are <20°, but could be dramatically enhanced to >120° when nanorough silicon 'black' substrates were used. Therefore, the substrate structure and morphology can be an important asset to control the wetting properties under light irradiation. This suggests that the molecular structure changes of a switchable organic monolayer are similarly important. Indeed, this has been demonstrated for self-assembled monolayers (SAM) of azobenzene alkane thiolates on Au surfaces. On flat surfaces, the photoswitches in a SAM can be closed packed when the growth and formation of the SAM are adjusted accordingly. However, the surface coverage of molecules inside the layer can have drastic consequences on their ability to change their structure under light irradiation. Moldt et al.[19] as well as Valley et al.[12] have studied the latter issue systematically and found for densely-packed layers of azobenzene moieties virtually no response to light irradiation in their photo-switching experiments, while 'diluted' SAMs exhibited a substantial switching ability. For light-responsive layers, steric hindrance is likely to impair the layer's ability to change their structure. In addition, to these intrinsic properties of a photo-switchable layer, also the presence of a vapor or a liquid phase can influence the switching ability and the switching kinetics quite substantially. This has been reported by Moldt et al.[9], who have studied azobenzene alkane thiols SAMs and compared the switching of the SAM in vacuum or in dry N_2 gas to the response of the same layer in ambient air that naturally contained water to some extent. In vacuum, the thermal life time of the Z configuration, which was prepared by irradiating the monolayers with UV light, was in the order of minutes but extended to more than one day in ambient air. From these observations, the authors concluded that the presence of water at the interface can stabilize the Z configuration and, thus, cause an increased thermal life time.[9] Because of slower thermal relaxation in ambient air, also the photostationary state is different and was significantly higher (~67 to 100 % Z) in ambient air in contrast to the situation in vacuum where photostationary states of the Z configuration were reported between 50 and 74 % Z.

In this paper, we report on the use of self-assembled monolayers with a new AAP derivative (Figure 1) that has a phosphonic acid headgroup and can be anchored to a α-Al_2O_3(0001) single crystal or any other aluminum oxide surface. Whereas many previous works have mostly concentrated on photo-responsive layers on silicon dioxide or Au surfaces using silanes or thiols, we discuss modification and

photoswitching at aluminum oxide surfaces which are of great technological importance. Particularly, we study the kinetic changes as well as the changes in the equilibrium surface structures by time-dependent vibrational sum-frequency spectroscopy (SFG), complementary dynamic contact angle measurements and simulations of the wetting behavior. The results that we provide exploit the connection between molecular changes at the interface and the dynamic changes in the macroscopic contact angle.

As remarkable and also unexpected result, it turns out that the processes within the photoswitchable substrate and at the drop side occur on comparable time scales and are, thus coupled to each other in a non-trivial manner. For that reason, we introduce a theoretical framework that allows one to predict the time-dependent change in the macroscopic contact angle and which is first verified by comparison with simulations of a model system and then applied for quantification of the experimental results. For that reason, we can add new information to open questions in adaptive and dynamic wetting.
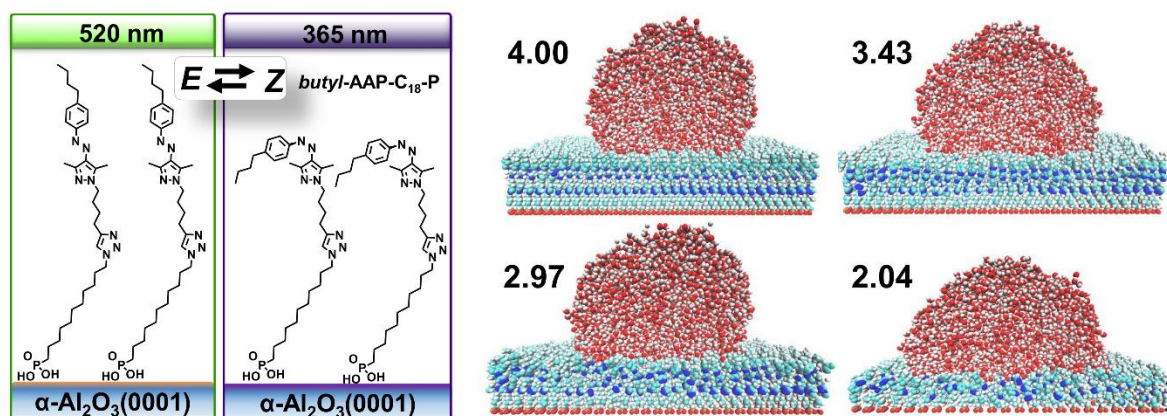
Figure 1. Structures of the E/Z configurations of butyl-AAP-C_{18} phosphonic acids which are deposited on α-$Al_2O_3(0001)$ surfaces. The AAP monolayer can be switched using light at wavelengths of 520 nm (green) and 365 nm (UV). Note that this is a rough sketch of possible E/Z monolayer structures on the substrate. Additionally snapshots from MD simulations are shown for a drop of water molecules on butyl-AAP-C_{18} phosphonic acids with different surface coverage. The surface coverage in units of molecules per nm² were as indicated in the figure.

4

METHODS AND EXPERIMENTAL DETAILS

Surface preparation and deposition of organic monolayers

α-Al_2O_3(0001) single crystals with a miscut of <0.1° were purchased from Impex HighTech (Germany). Prior to the deposition of AAP monolayers the α-Al_2O_3(0001) surfaces were cleaned in a 80 °C piranha solution for 30 min and two times in an alkaline cleaning solution (1:1:5, NH_3 (25%): H_2O_2 (35%): H_2O) at 80 °C for at least 30 min. Immediately before depositing the monolayers, the substrates were removed from the cleaning solution and were extensively rinsed with ultrapure water and subsequently dried in a stream of nitrogen gas (>99.999 %, Westfalen). Ultrapure water (total organic carbon <5 ppb, 18.2 MΩcm) was obtained from a Millipore Reference A+ purification system and was used also as a subphase for Langmuir-Blodgett deposition of AAP monolayers. Synthesis of the *butyl*-AAP-C_{18} phosphonic acid (Figure 1) and the Langmuir-Blodgett transfer[27] of the monolayers to the α-Al_2O_3(0001) single crystals were done as described in detail in the Supporting Information. Photoswitching of the monolayers was done similarly in all experiments using LEDs with wavelengths of 520 nm (Roschwege, LSC-G) and 365 nm (Roschwege, Star-UV365-05-00-00) and by irradiating the samples with a different fluence that was adjusted to values between ~1.1 and 5 mWcm^{-2} at a wavelength of 520 nm and between ~1.25 and 7 mWcm^{-2} at a wavelength of 365 nm. In the results and discussion part, we will address the fluence dependence in detail. Contact angle goniometry was done using a Krüss DSA 100 (Germany) device that was equipped with a homebuilt cell for *in situ* irradiation of the samples with green and UV light. This cell was equipped with two OG 590 long-pass filters (Schott, Germany) to exclude additional influences from the ambient room light and from the goniometers white light source. The cell was continuously purged with nitrogen gas that was bubbled through ultrapure water in order to increase the relative humidity of the vapor phase to >90 % and to minimize evaporation of the sessile drop during contact angle measurements. Sessile drops with a volume of 10.2±0.14 μL and 20.37±0.02 μL were deposited onto the surfaces and the collection of data was immediately started. *In situ* irradiation of the samples in the contact angle goniometer with UV and green light was done with the light sources noted above. For that, both LEDs were integrated in the measurement cell.

Broadband vibrational sum-frequency generation spectroscopy (SFG)

Vibrational sum-frequency generation spectroscopy (SFG) is a second-order nonlinear spectroscopy that is broadly applied to study surfaces and interfaces.[28–30] Sum-frequency photons are generated by two high intense laser beams: a frequency-tunable IR beam (ω_{IR}) and a second beam at a fixed frequency (ω_{vis}). Both beams are overlapped in time and space at an interface, where they generate a third beam with the sum frequency (SF) $\omega_{SF} = \omega_{IR} + \omega_{vis}$ of the two incoming beams. The SFG intensity is directly proportional to the square of the effective second-order electric susceptibility, which is given as the sum of a nonresonant contribution $\chi_{NR}^{(2)}$ and resonant contributions $\chi_{R}^{(2)}$:[28,31–33]

$$I_{SF} \propto \left| \chi_{NR}^{(2)} + \sum_q \frac{A_q e^{i\varphi_q}}{\omega_{IR} - \omega_q + i\Gamma_q} \right|^2 \tag{1}$$

While $\chi_{NR}^{(2)}$ is dominated by electronic excitations at the interface, $\chi_{R}^{(2)}$ originates from molecular vibrations of interfacial molecules that can be resonantly excited by the incoming IR pulse.

A_q, ω_q, φ_q and Γ_q are the amplitude, the resonance frequency, phase (relative to $\chi_{NR}^{(2)}$) and homogenous line width of the qth vibrational mode. The amplitude $A_q = N \left\langle \beta_q^{(2)} \right\rangle$ is a function of the surface excess of adsorbed molecules N and a function of the orientational average $\langle ... \rangle$ of the molecular hyperpolarizability $\beta_q^{(2)}$. While $\beta_q^{(2)}$ is linearly dependent on the Raman polarizability and the dynamic dipole moment of the vibrational mode, its orientational average has far reaching consequences for isotropic materials or materials with inversion symmetry where the orientational average is zero in the bulk material but necessarily nonzero at an interface. This makes SFG spectroscopy an inherently surface-selective method for these materials.

The home-built setup of our broadband SFG spectrometer is described in detail elsewhere.[34] In brief, it consists of a chirped pulse regenerative amplifier (Spectra Physics Solstice Ace, USA) which produces 70 fs pulses at a center wavelength of 795 nm. 3.4 mJ of the available pulse energy was used to pump an optical parametric amplifier (Light Conversion TOPAS Prime, Lithuania) with a separate unit for noncollinear difference frequency generation. The tunable broadband femtosecond pulse in the mid-IR had a spectral bandwidth of >300 cm^{-1} and was overlapped with a time-asymmetric picosecond pulse at a wavelength of 804.1 nm that had a bandwidth of <5 cm^{-1}. The vis and the IR pulse were focused at the

sample with incident angles of 55° and 60° with respect to the surface normal. Here, beam diameters of 530 and 260 μm were established and both pulses overlapped in time and in space. To avoid possible radiation damage by the intense laser pulses, the pulse energies of vis and IR beams were both reduced to 15 μJ. SFG signals were collected in a reflection geometry and guided to the detection system that consisted of an Andor Kymera (Oxford Instruments, UK) spectrograph equipped with a 1200 lines/mm grating and an Andor Newton EMCCD that detected SFG photons with high efficiency. SFG spectra were recorded in this study by using a single IR center frequency and, thus, without tuning the IR pulse in order to reduce the time needed to acquire SFG spectra that was particularly important for the time-dependent experiments. For equilibrated samples, very long acquisition times of up to 120 s were possible, while for samples far from equilibrium rapid acquisition of SFG spectra was required and the acquisition times varied between 1 and 10 s depending on the time constants of the switching processes (on which we will report in detail below). In order to increase the signal-to-noise (S/N) ratio of the SFG spectra when fast acquisition of spectra was required (e.g. 0.5 s per spectrum), we have performed the experiments on the switching kinetics up to 10 times. Subsequently, the SFG spectra were averaged from the different but identically performed kinetic runs during the $E \rightarrow Z$ (UV irradiation) and the $Z \rightarrow E$ (green irradiation) switching processes. This procedure resulted in a significantly improved S/N ratio. All SFG spectra were taken at s-polarized sum-frequency, s-polarized visible and p-polarized IR beams (ssp). SFG spectra taken at other polarization combinations are presented in the Supporting Information. All SFG spectra were normalized to the nonresonant SFG spectrum of an air-plasma cleaned thin gold film that was deposited on a silicon wafer.

Atomistic simulations of the molecular system

In order to investigate the interaction of the substrate with water molecules, we have performed molecular dynamic simulations for substrates with molecular monolayers that had different packing densities. For the simulations we used the package GROMACS[35] and the generalized Amber force field.[36] *Butyl*-AAP-C$_{18}$ phosphonic acids (Figure 1) were placed in a rectangular simulation box with dimensions in x- and y-directions that were slightly dependent on the studied system but were not smaller than 16 nm and 5.4 nm, respectively. The restrained electrostatic potential (RESP) charges of the AAP molecules were calculated from the ESP charges using Antechamber.[37] Therefore the geometry

of the molecule was optimized with Gaussian16 using a 6-31G(d) basis set.[38–41] Afterwards the ESP charges were determined with a Hartree Fock calculation. Periodic boundary conditions were present in x- and y-direction while in z-direction the box was limited by an implicit wall. To calculate the interaction between the wall and the atoms a Lennard-Jones 9-3 potential was used. Since the walls should just kept the particles inside the simulation box, we chose a relatively small self-interaction parameter for the wall atoms of $\varepsilon_{WL} = 10^{-5}$ kJ mol^{-1} and a wall number density of $\rho_{wall} = 0.01$ nm^{-3}. The phosphonic acid groups of the molecules were frozen in order to keep the molecules on their place. The time step was set to 2 fs and the cutoff for van-der-Waals as well as for Coulomb interactions was set to 1.5 nm. Beyond this cut off Coulomb interactions were calculated with the smooth particle mesh Ewald (SPME) method[42] with a correction for slab geometries.[43] We used a v-rescale thermostat[44] in order to keep the temperature of the system at 300 K. The parallel linear constraint solver (LINCS) algorithm[45] was used to kept hydrogen bonds constrained. An already equilibrated droplet consisting of $8 \cdot 10^3$ TIP3P water[46] molecules was placed on the surface and the system was equilibrated for 10 ns before snapshots were rendered with VMD.[47]

Model simulations of the dynamical aspects of wetting

Our model system consists of two types of particles, the substrate particles (denoted with 's') which are frozen and arranged in two layers of a fcc(111) lattice and the fluid particles (denoted with 'l'). All particles interact through the Lennard-Jones potential

$$V(r_{ij}) = 4\varepsilon_{ij}\left(\left(\frac{\sigma_{ij}}{r_{ij}}\right)^{12} - \left(\frac{\sigma_{ij}}{r_{ij}}\right)^{6}\right) \qquad (2)$$

where r_{ij}, ε_{ij} and σ_{ij} are the distance between particles i and j, the interaction strength between both particles calculated as the geometric mean of the self-interaction parameters ε_i and ε_j and the arithmetic mean of their diameters r_i and r_j, respectively.

By varying the self-interaction parameter of the substrate ε_s (note that the interaction between fluid and substrate particles is $\varepsilon_{sl} = \sqrt{\varepsilon_s}$ since we set $\varepsilon_l = 1$) we can change the wettability of the substrate. The potential is truncated and shifted at a cutoff-radius of $r_c = 2.5\,\sigma$. The system is simulated in a NVT ensemble with the package HOOMD.[48] We set all particle diameters $\sigma_s = \sigma_l = \sigma$ as well as the mass

$M = 1$. The temperature, which is controlled by a dissipative particle dynamics (DPD) thermostat[49,50] is $\frac{k_B T}{\varepsilon_l} = 0.75$ and the time step $\tau = (200\,\sigma)^{-1}\sqrt{\varepsilon_l/M}$. The system has periodic boundary conditions in x- and y-direction. In our simulations we use a total amount of $N = 4 \cdot 10^4$ fluid particles. Every simulation setup is averaged over 50 trajectories. To obtain the contact angles of our droplets we average the density field of the fluid particles along the y-coordinate and calculate the position of the liquid-vapor interface for different slabs in z-direction with the function

$$\rho_z(x) = \frac{1}{2}(\rho_l + \rho_g) - \frac{1}{2}(\rho_l - \rho_g)\tanh\left(\frac{2(x - x_\beta(z))}{d_\beta}\right) \qquad (3)$$

where $\rho_z(x))$ is the density of the fluid at position x in slab z, ρ_l and ρ_g are the density of the fluid at position x, in the liquid and in the gas phase, respectively, x_β is the position of the interface and d_β is the width of this interface. The obtained values can be fitted with a circle and the contact angle is calculated from this fit.

Analytical model of the wetting dynamics for time-dependent surface tension

First, we want to address the dynamic contact angle by using an adaptation model for the interfacial energies which has been discussed in detail by Butt et al.[4]. In our work, we can make use of the advantage of having a single layer of molecules which reduces the complexity as opposed to e.g. polymer brushes and the fact that we actually determine the characteristic times for photo-switching on a molecular level from SFG spectroscopy (see below). For modeling, we can assume first-order kinetics where we use the effective rate constant $k_e^{E \to Z} = \frac{1}{\tau_{E \to Z}}$. To describe the dynamic contact angle, one can use the known Young equation that describes the contact angle as a function of the interface tensions γ_L, γ_S and γ_{SL} which arise from the liquid-gas, solid-gas and the solid-liquid interfaces:

$$\gamma_L \cos\Theta_\infty = \gamma_{S,\infty} - \gamma_{SL,\infty} \qquad (4)$$

Furthermore we are neglecting the influence of gravity and adaptation of the drop and, correspondingly, assume that the water molecules in the drop follow the transient changes in interface chemistry instantaneously. This assumes that the drop is always instantaneously equilibrated to the change in interface chemistry. This oversimplifies the processes during dynamic wetting and we will come back

to this issue below. In eqn. (5) the index "∞" indicates values of the interface tension and of the contact

angle after switching and sufficient (infinite) long waiting times. As the photo-switchable layer can

change the interface tension at the solid-liquid as well as at the solid-gas interface we write:

$$\gamma_{SL} = \gamma_{SL,\infty} + \Delta\gamma_{SL}\, e^{-\frac{t}{\tau_{E\rightarrow Z}}} \qquad (5)$$

and

$$\gamma_S = \gamma_{S,\infty} + \Delta\gamma_S\, e^{-\frac{t}{\tau_{E\rightarrow Z}}} \qquad (6)$$

Inserting eqns. (5) and (6) into Youngs equation (7)

$$\gamma_L \cos(\Theta(t)) = \gamma_S - \gamma_{SL} \qquad (7)$$

and by rearranging and simplifying the result using eqn. (4) we get:

$$\cos(\Theta(t)) = \cos\Theta_\infty - \left(\frac{\Delta\gamma_{SL} - \Delta\gamma_S}{\gamma_L}\right) e^{-\frac{t}{\tau_{E\rightarrow Z}}} \qquad (8)$$

We note that from eqn. (8) we expect that the change $d\cos(\Theta(t))/dt$ very shortly after time zero is

nonzero. Furthermore, since in this model we only consider the switching of the substrate, we implicitly

assume that the liquid is at a given time always instantaneously equilibrated to the new interface energies

(eqns. (7) and (8)).

Next, we generalize this picture by taking into account the finite relaxation behavior of the liquid in the

presence of a time-dependent surface tension. In the molecular kinetic theory of wetting[51] the driving

force is the deviation of the free energy from the equilibrium value. This free energy difference can be

expressed by the difference of the cosine of the contact angle to its equilibrium value. The driving force

yields a finite velocity of the contact line which, for fixed volume of the droplets, gives rise to a variation

of the contact angle. In case of an infinitely fast switching process, this can be most generally written as

$$\frac{d}{dt}\cos(\Theta(t)) = -k\big(\Theta(t)\big)[\cos(\Theta(t)) - \cos(\Theta_{eq})] \qquad (9)$$

The factor $k(\Theta)$ involves the kinetic factors as well as the relation between the contact angle and the

width of the droplet for fixed volume of the droplet and typically under the assumption of spherical

symmetry. However, for small variations of the contact angle we can neglect the Θ −dependence of the prefactor k. In this way the relaxation process, as measured by $\cos(\Theta)$, is a simple exponential with the relaxation rate k. Indeed, as shown below, this is a very good approximation if compared with the simulated data in the limit of fast switching. Actually, even for different approaches for the driving force such as the use of the Cox-Voinov law,[52,53] the linear eqn. (10) would remain valid as long as the change in contact angle is small.

This approach allows us to take into account the time-dependence of the switching process by choosing a time-dependent equilibrium angle, i.e. $\Theta_{eq}(t)$, yielding

$$\frac{d}{dt}\cos\big(\Theta(t)\big) = -k[\cos(\Theta(t)) - \cos(\Theta_{eq}(t))] \quad . \quad (10)$$

To simplify the description, we furthermore introduce the normalized contact angle

$$x(t) = \big(\cos\big(\Theta(t)\big) - \cos\Theta_f\big)/\big(\cos\Theta_i - \cos\Theta_f\big) \quad (11)$$

with Θ_i the initial contact angle at time zero and Θ_f the final contact angle when the system has reached the new equilibrium. With these variables, and assuming an exponential approach of the substrate properties towards its final state upon switching, we can express the cosine of the time-dependent equilibrium angle as (using $k_e = \frac{1}{\tau_{E \to Z}}$)

$$\cos\big(\Theta_{eq}(t)\big) = \cos\big(\Theta_f\big) + \big(\cos\Theta_i - \cos\Theta_f\big)e^{-k_e t} \quad (12)$$

Note that we introduced two independent relaxation rates: k for the relaxation of the liquid (in the limit of a fast switching process) and k_e for the relaxation of the substrate. Then we can simplify eqn. (10) as:

$$\left(\frac{d}{dt}\right)x(t) = -k[x(t) - e^{-k_e t}] \quad (13)$$

with the initial condition $x(0) = 1$. This inhomogeneous differential equation can be easily solved, yielding for $k \neq k_e$

$$x(t) = -\frac{k_e}{k - k_e}e^{-kt} + \frac{k}{k - k_e}e^{-k_e t} \quad , \quad (14)$$

thereby fulfilling the initial condition. For the special case $k = k_e$ one would obtain $x(t) = (1 + kt)\, e^{-kt}$.

When estimating the effective characteristic time τ_{eff} as $\int x(t)\, dt$ one obtains after a short calculation the relation

$$\tau_{eff} = \frac{k^2 - k_e^2}{k k_e(k - k_e)} = \frac{k + k_e}{k k_e} = \tau + \tau_e \qquad (15)$$

where the relaxation times are the inverse of the respective relaxation rates. Furthermore, it turns out that $\left(\frac{d}{dt}\right) x(t = 0) = 0$ for all combinations of k and k_e, which is largely different from a simple exponential relaxation process. At this point we note that eqn. (15) is symmetric upon exchange of k and k_e. This is a remarkable result as both rates are of very different molecular origin.


RESULTS AND DISCUSSION

UV\Vis spectroscopy of bulk molecules and their switching ability

In Figure 2a, UV\Vis spectra of the *butyl*-AAP-C$_{18}$ phosphonic acids are shown where the molecules were dissolved in chloroform and which report on the response of the isolated molecules in a solvent that does only weakly interact with the molecule as we will discuss below. For samples that were irradiated with green light or after thermal equilibration under dark condition, the UV\Vis spectra show a strong $\pi \rightarrow \pi^*$ band at 337 nm. In addition, a weaker n $\rightarrow \pi^*$ band at ~427 nm is noticeable. For samples that were irradiated by UV light, the absorbance of the $\pi \rightarrow \pi^*$ band decreased substantially and was blue-shifted to ~315 nm, whereas the n $\rightarrow \pi^*$ band increased in absorbance and was red-shifted to ~448 nm.

Clearly, the molecules do switch to a large extend. From previous work,[18] it is known that the switching kinetics of isolated molecules in the bulk are largely different to the interfacial kinetics. For that reason we want to focus here on the thermal stability of the *Z* configuration in two different solvents as this is also of great interest for the molecular changes and wetting dynamics of *butyl*-AAP-C$_{18}$ phosphonic acid monolayers. In Figure 2b, we present the change in absorbance of *butyl*-AAP-C$_{18}$ at a wavelength of 337 nm which interrogates the $\pi \rightarrow \pi^*$ band as a function of time after the samples were irradiated with

UV light and, thus, the *Z* form was predominant. Consequently, the increase in absorbance with time, while samples are kept under dark conditions, reports on the thermal relaxation from the *Z* to the *E* configuration and can be used to determine the thermal stability of the *Z* configuration. Clearly, the effect of the solvent on the thermal stability is dramatic: In chloroform already after 10 to 20 min the *butyl*-AAP-C_{18} phosphonic acid molecules relax back to the *E* form and thermal equilibrium was reached, while for methanol the time scale of the thermal relaxation is drastically different. The thermal stability of the *Z* isomer is several orders of magnitude higher and it takes days for the molecules to thermally relax from the *Z* into the *E* configuration (Figure 2b). We have to note that similar experiments of the molecules dissolved in water would be highly interesting, but the solubility in water was too poor to conduct these experiments.
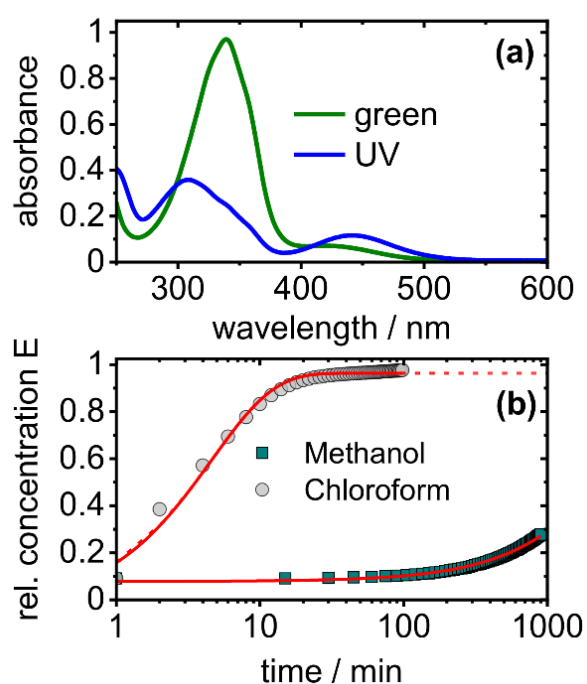
Figure 2 *(a) UV/Vis spectra of butyl-AAP-C_{18} phosphonic acid with a concentration of 0.1 mM in chloroform as a solvent and for prolonged irradiation with 365 nm UV light (blue line) and 520 nm green light (green line). (b) Thermal stability of the Z isomer as inferred from the absorbance at a wavelength of 337 nm for 0.1 mM butyl-AAP-C_{18} phosphonic acid in chloroform (circles) as well as in methanol (squares) while the solutions were kept in the dark.*

However, we can already draw an important conclusion from the results in Figure 2b: The drastically different thermal stabilities of *butyl*-AAP-C$_{18}$ phosphonic acid moieties in chloroform and methanol are attributed to a stabilization of the *Z* state possibly through hydrogen bonding of the methanol's O-H group with the exposed azo group of the *Z* configuration. At this point, we can hypothesize that the effects of H$_2$O on the stabilization of the *Z* state might be even more pronounced.

Photo-switchable AAP monolayers in equilibrium

In Figure 3 we present SFG spectra of α-Al$_2$O$_3$(0001) surfaces that were coated with a monolayer of *butyl*-AAP-C$_{18}$ phosphonic acids (see SI) using the Langmuir-Blodgett[27] technique. For all SFG experiments as well as the wetting experiments we have adjusted the coverage of the photoswitches on the α-Al$_2$O$_3$(0001) surface to 6.7±0.5 molecules/nm^2 (14.8±1.2 Å^2), because this coverage has resulted in the largest switching ability of the layer in terms of relative changes in the SFG spectra which is discussed in some detail in the Supporting Information. Furthermore, the MD simulation shows that at a density of 4 molecules/nm², wetting of the *butyl*-AAP-C$_{18}$ phosphonic acids layer with water does not lead to substantial restructuring of the layer when the molecules are in their *E* configuration (Figure 1). This is different for instance at much lower coverage of 2.04 molecules/nm² where a substantial restructuring of the monolayer in the presence of the water drop is observed.

We recall that earlier works[12,19,54] with azobenzene derivatives have shown that steric hindrance in closed-packed layers may prevent or severely reduce the ability of the layer for *E*/*Z* photoisomerization and, consequently, one has to compromise between the switching ability and sufficient surface coverage. Although the connection between switching ability and surface coverage is an interesting aspect, we concentrate here on the molecular structure changes of the *butyl*-AAP-C$_{18}$ phosphonic acids on the aluminum oxide substrate as a function of light irradiation in relation to their wetting dynamics.

For that we need in depth information on the layers' kinetic changes after the light irradiation is changed and when the interfaces are far from their equilibrium.

We point out that previous works[13,18] have shown that arylazopyrazole derivatives e.g. in an aqueous solution exhibit the largest changes and the highest photostationary states for *Z*→*E* switching when 520 nm visible light was used, while for *E*→*Z* switching UV light e.g. at a wavelength of 365 nm is necessary.
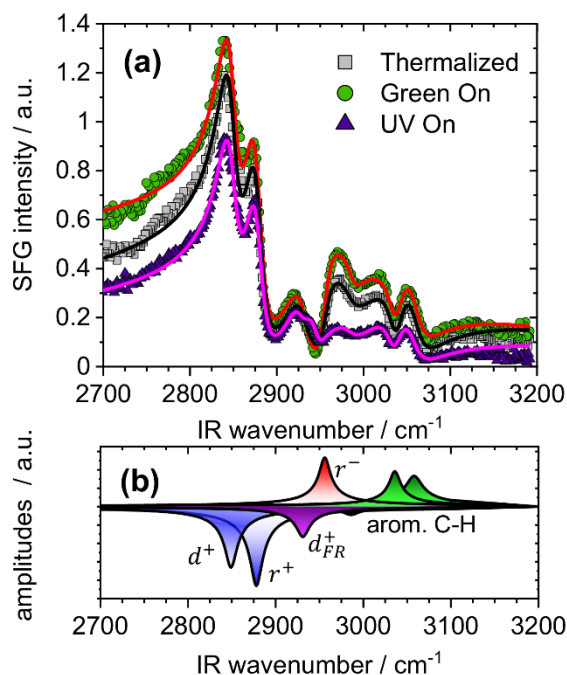
Figure 3. (a) Vibrational SFG spectra of butyl-AAP-C_{18} phosphonic acid monolayers with a coverage of 6.7±0.5 molecules/nm² (14.8±1.2 Å² per molecule) on α-Al_2O_3(0001). Depicted are spectra for three states of the monolayer: Two spectra for predominant E configuration of the molecules which was either achieved by prolonged and continuous irradiation with 520 nm light (green circles) or by thermally equilibrating the sample in the dark for 15 h (grey squares). Furthermore the SFG spectrum of molecules predominantly in their Z configuration is shown. This state was established by prolonged and continuous irradiation with 365 nm UV light (dark blue triangles). Solid lines correspond to nonlinear least square fits to the spectra as explained in the main text. (b) SFG amplitudes of the individual bands decomposed from the spectrum (green on) in (a). For further information on the fitting procedures and the fit parameters the reader is referred to the Supporting Information.

For that reason, we have applied light irradiation at these two specific wavelengths to drive the molecular changes in the *butyl*-AAP-C_{18} phosphonic acid monolayers. The SFG spectra in Figure 3 were recorded under continuous irradiation with either green light (*E* state) or UV light (*Z* state), respectively, and after the α-Al_2O_3(0001) surfaces with *butyl*-AAP-C_{18} phosphonic acid monolayers were brought into an equilibrium. This was achieved by prolonged exposure to green or UV light.

Once, equilibrium was reached the changes in the SFG spectra as a function of time were negligible. Figure 3a presents the SFG spectrum of a *butyl*-AAP-C_{18} phosphonic acid monolayer with the molecules in their *E* configuration (Figure 1) which shows a rather complex shape with a substantial non-resonant contribution $\chi_{NR}^{(2)}$ that heterodynes the resonant contribution and causes the apparent dispersive line shapes and the 'offset' in SFG intensity that is best seen at the low frequency side of the SFG spectra

(2700 to 2800 cm^{-1}). The fact, that photoswitchable molecules as well as dye molecules can exhibit a strong $\chi_{NR}^{(2)}$ contribution is well-known and has been discussed in several previous works which have mostly concentrated on air-water interfaces that were decorated by these molecules. For instance, Bonn and co-workers[55] investigated photoswitchable lipids at the air-water interface and found similarly strong $\chi_{NR}^{(2)}$ contributions, while Schnurbus et al.[18] could additionally show for AAP amphiphiles that $\chi_{NR}^{(2)}$ is proportional to the surface excess of the AAP surfactants at the air-water interface. Schnurbus et al.[18] related the relatively high $\chi_{NR}^{(2)}$ to the fact that the SFG wavelength of 650 nm is close to the optical transitions of the AAP moieties which can be switched efficiently at 520 nm. Therefore $\chi_{NR}^{(2)}$ is much higher as for optically transparent systems where the SFG wavelength is far away from optical transitions. In order to compare $\chi_{NR}^{(2)}$ for E and Z configurations, we first concentrate on the low frequency side of the SFG spectra in Figure 3, where a close inspection reveals a much lower $\chi_{NR}^{(2)}$ for the Z compared to the E state and where we can again use the apparent offset at 2700 - 2800 cm^{-1} in the SFG spectra as an estimate of the non-resonant contribution to the second-order electric susceptibility $\chi_{NR}^{(2)}$. The reduction of $\chi_{NR}^{(2)}$ can be directly related to the electronic modification of the AAP moieties when they are switched from the E to the Z configuration. For example, this is seen as drastic changes in the absorbance spectra (Figure 2a). Clearly, the optical transitions of the Z configuration are more separated from the SFG wavelength and thus the differences in the relative strength of $\chi_{NR}^{(2)}$ for the molecules in their E/Z state can be directly related to the number density of molecules that become switched and thus electronically modified. In addition to $\chi_{NR}^{(2)}$ contributions, we observe distinct vibrational bands in the SFG spectra at 2853 and 2880 cm^{-1} which we attribute to symmetric stretching vibrations of methylene (d^+) and methyl (r^+) groups, whereas the bands at 2925, 2944, 2949 and 2986 cm^{-1} arise from CH$_2$ (d_{FR}^+) and CH$_3$ (r_{FR}^+) Fermi resonances, CH$_3$ antisymmetric stretching (r^-) and CH$_2$ antisymmetric stretching (d^-) vibrations and, respectively.[56–58] Additional bands at 3036 and 3058 cm^{-1} can be noticed in Figure 3 and are attributed to aromatic C-H stretching vibrations at the aromatic[59] and at the triazole groups of the *butyl*-AAP-C$_{18}$ phosphonic acid monolayer, respectively. All bands are observed for both E and Z configurations, but E/Z photoisomerization of the *butyl*-AAP-C$_{18}$ phosphonic

acid monolayer causes an overall decrease in SFG intensity which can be associated to a decrease in $\chi_{NR}^{(2)}$ but also to a change in the amplitude of the resonant r^- contributions.

At this point we note that the SFG spectra show a relatively strong d^+ band, which is expected to be fairly small if all alkyl chains of the molecules in the monolayer are in their *trans* state without a high concentration of gauche conformations. Since this is obviously not the case and the strong d^+ band was observed independent of the surface pressure used during Langmuir-Blodgett transfer of the layer (Supporting Information) we take the strength of the d^+ band relative to the r^+ band as a qualitative indicator for the presence of gauche conformations in the undecyl chain from the phosphonic acid anchor to the triazole group of our monolayer (see Figure 1). This is consistent with earlier works,[60–62] where self-assembled monolayers of alkyl phosphonic acids with different chain lengths (C_8 to C_{18}) were studied on aluminum oxide as well as on other interfaces. The lateral attractive van der Waals interactions in monolayers are only in the presence of very long alkyl chains e.g. for octadecyl phosphonic acids sufficiently high enough to drive the alkyl chains in an *all-trans* configuration, while in other systems with shorter alkyl chains ($<C_{18}$), gauche conformations were present. In order to analyze the apparent changes in the SFG spectra in Figure 3 in more detail, we have performed non-linear least square fits to the spectra using model function with Lorentzian line shapes (eqn. (1)). For that we have initially fitted the SFG spectrum of the sample with the molecules in their *E* configuration allowing all parameters (A_q, ω_q, and Γ_q) to vary within limits. In the Supporting Information we provide the full parameter sets used for fitting the spectra in Table S1.

At this point the exact numbers are not relevant for the discussion, where we concentrate only on their relative changes. Using the fitted spectrum for the *E* configuration as a starting point, we have also fitted the SFG spectrum of the molecules in their *Z* state. This was done by allowing only the amplitudes of the vibrational bands and $\chi_{NR}^{(2)}$ to vary. In fact, the amplitudes of the r^- changed together with the $\chi_{NR}^{(2)}$ contribution (Supporting Information, Table S1), while the changes of the other bands were very small (SI). These changes are in contrast to the d^+ and r^+ bands which do not change with light irradiation and which we, thus, relate mostly to the residual part of the molecules that is located below the azo group and which is not changing orientation during *E/Z* photoisomerization (see again Figure 1).
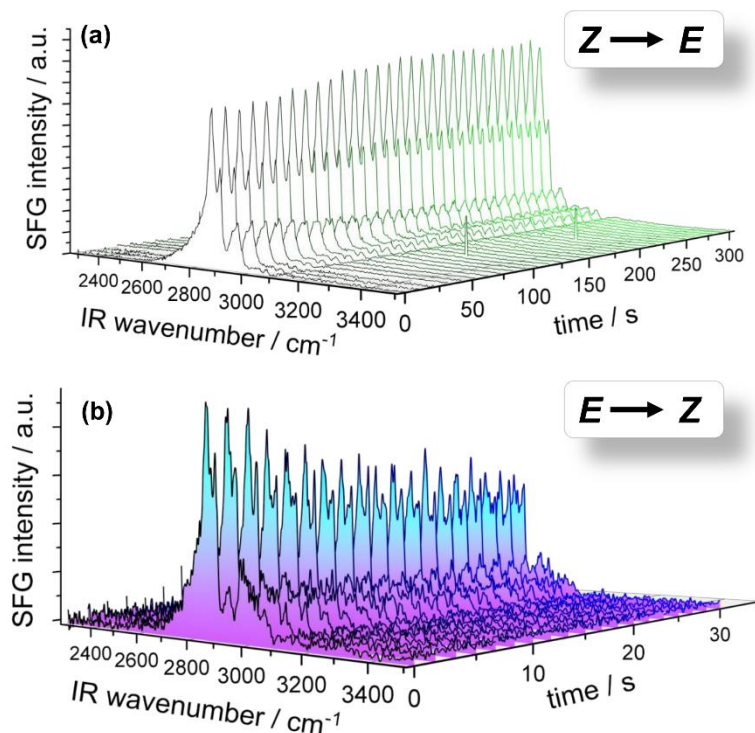
Figure 4. *(a) Time-dependent SFG spectra for Z→E switching of a butyl-AAP-C₁₈ phosphonic acid monolayer on α-Al₂O₃(0001) after changing the light irradiation from 365 nm UV to 520 nm green light (1.1 mW/cm²) at t=0 s. (b) Time-dependent SFG spectra for E→Z switching of the monolayer after the irradiation was switched from green to UV light (2.5 mW/cm²) at t=0 s.*

Photo-switching kinetics of *butyl*-AAP-C₁₈-P monolayers on α-Al₂O₃(0001)

To address also non-equilibrium properties and the switching of the monolayer at the molecular level, we have additionally performed time-dependent SFG spectroscopy that is capable of tracking the switching kinetics *in situ*. For that, we have first equilibrated the samples through prolonged irradiation with 520 nm green light which establishes the *E* configuration of the molecules in the monolayer and, subsequently, switched the light source from green to 365 nm UV light within <1 s. This triggers the *E→Z* configurational change within the monolayer and was done while SFG spectra were continuously recorded at a rate of one spectrum per second. This has allowed us to track the changes in molecular structure during the transition from one equilibrium structure to the other. Once a new equilibrium was reached, the light irradiation was again switched but now from UV to green light, while the integration per SFG spectrum was increased to 10 s and consecutive SFG spectra were recorded until the sample

was equilibrated again. This procedure was repeated up to 10 times and the SFG spectra from each switching half cycle were averaged to increase the S/N ratio as explained in the experimental details part. The results of these experiments with the samples in a non-equilibrium state are presented in Figure 4. Clearly, the changes in the SFG spectra during the *E/Z* photo-isomerization of the AAP moieties are within a few seconds for $E{\rightarrow}Z$ switching and a few minutes for $Z{\rightarrow}E$ switching, while the overall changes in the SFG spectra from one equilibrium state to the other are consistent to what is shown in Figure 3. In order to analyze the dynamic changes in the spectra in Figure 4 quantitatively, we have first integrated the off-resonance intensity at the low frequency side (<2800 cm^{-1}) of the SFG spectra in Figure 4, which we take as a reference for the changes in the non-resonant contribution $\chi_{NR}^{(2)}$. As we have already discussed in the previous section the apparent changes of the d^+ and r^+ bands are only caused by changes in $\chi_{NR}^{(2)}$ contributions, whereas the amplitude of the r^- band does also change with *E/Z* configuration (see Table S1 and Figure S4 in SI). The latter is also seen by a close inspection of Figures 4a and 4b where the intensity change of the r^- band closely follows the change of $\chi_{NR}^{(2)}$ in time. Since $\chi_{NR}^{(2)}$ provides information on the modifications in the electronic structure of the AAP moieties, while the resonant contributions report on the structural changes of the monolayer, it is interesting to discuss whether the changes in electronic and molecular structure are actually synchronized. For that reason, we have additionally fitted the SFG spectra in Figure 4 with model functions according to eqn. (1) and plot the amplitudes of the $\chi_{NR}^{(2)}$ and the r^- contributions as a function of time in Figure S4 of the Supporting Information, while we show in Figures 5a and 5b the integrated SFG intensity proportional to $\left|\chi_{NR}^{(2)}\right|^2$ as a function of time and for $Z{\rightarrow}E$ and $E{\rightarrow}Z$ switching, respectively.

In order to gain information on the characteristic times for each transition we have fitted the dynamic changes in SFG intensity and amplitude (Figures 5 and S4) assuming first-order kinetics

$$C(t) = C_0 + C_\infty\left(1 - e^{-k_e\,t}\right) \qquad (16)$$

where $C(t)$ correspond to the change in SFG signal or non-resonant contribution for $E{\rightarrow}Z$ or $Z{\rightarrow}E$ switching and k_e is an effective rate constant for the switching process with $\tau = k_e^{-1}$ the corresponding characteristic switching time. The characteristic switching times that we can derive from the effective rate constants by fitting the results in Figures 5a and 5b using eqn. (16) are for $\tau_{E{\rightarrow}Z}$ equal to ≈1 s, 4 s,

8 s and 15 s when the light intensity at 365 nm irradiation was adjusted to 7, 5, 2.5 and 1.25 mW/m², respectively. Thus, $\tau_{E \to Z}$ varies linearly with the light intensity, while the characteristic time $\tau_{Z \to E}$ of the reverse process was in the range of 167 to 237 s and did not vary linearly with light intensity at 520 nm when the latter was varied between 1.25 and 5 mW/cm² (Table 1).

Before we discuss the dependence on the light irradiance of the light source, we come back to the earlier question if the electronic and molecular structure changes are synchronized. For that, we compare the kinetic changes of $\chi_{NR}^{(2)}$ and r^- contributions in Figure S4 (Supporting Information), and determine the characteristic times for E/Z switching separately for the nonresonant contribution and the r^- resonant contribution. In fact, we can model the time dependence of both amplitudes with the identical time constant that was also used to fit the intensity-based data. Consequently, we can conclude that within the experimental scatter both electronic and structural changes of the AAP monolayers are indeed synchronized. The excellent overlap between the two approaches brings also strong support to our analysis of the integrated intensities, from which we expect smaller errors as the signal-to-noise ratio of results is significantly higher (e.g. compare Figures 5b and S4d).

The rate constant k_e must be dependent on the irradiance of the light source I, the absorbance of the sample $\alpha(\lambda)$ and the wavelength λ that is used to trigger the E/Z photoisomerization within the monolayer.

From these characteristic times or effective rate constants, we cannot directly infer the intrinsic rate constants $k_e \propto k_i \frac{hc_0}{\lambda} \alpha I$ for E/Z photoisomerization of the butyl-AAP-C$_{18}$ phosphonic acid monolayers. However, we can use the ratio

$$\frac{\tau_{E \to Z}}{\tau_{Z \to E}} = \frac{k_e^{Z \to E}}{k_e^{E \to Z}} = \frac{k_i^{Z \to E}}{k_i^{E \to Z}} \frac{I_{520} \, \alpha_{520} \lambda_{365}}{I_{365} \alpha_{365} \lambda_{520}} \qquad (17)$$

to provide a better comparison of the intrinsic switching kinetics of the E/Z photoisomerization. For that we are using the absorbance at a wavelength of 520 and 365 nm which we can determine to 0.145 and 0.875, respectively, from the results shown in Figure 2. Further, we use a fluence of 2.5 mW/cm² for

both the green as well as the UV LED light sources to determine the ratio of the intrinsic rate constants from effective rate constants (or alternatively the effective characteristic times):

$$\frac{k_i^{Z \to E}}{k_i^{E \to Z}} = \frac{\tau_{E \to Z}}{\tau_{Z \to E}} \frac{I_{365} \alpha_{365} \lambda_{520}}{I_{520} \alpha_{520} \lambda_{365}} = 0.011 \qquad (18)$$

Using this relation, we can also express the intrinsic switching times as the inverse of the intrinsic rate constants and obtain accordingly: $\tau_i^{Z \to E} \approx 91 \cdot \tau_i^{E \to Z}$
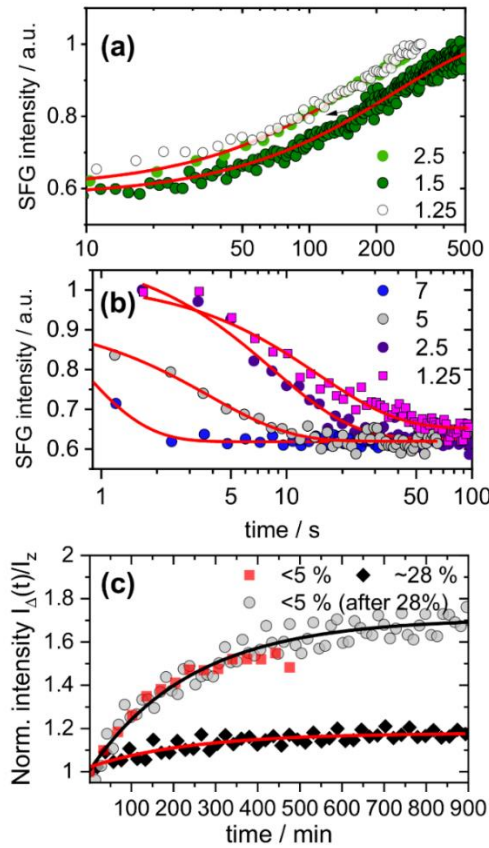
Figure 5 *(a) and (b) present the integrated SFG intensity of the resonant and nonresonant contributions as a function of time after irradiation with green and UV light was initiated at t=0 s, respectively. For (a) the samples were at t<0 s irradiated with UV light and t>0 s with green light while for (b) the samples were irradiated with UV light t<0 s which was switched at t>0 s to green light until equilibrium was reached. The legend indicates the light intensity in mW/cm². (c) Presents the stability of the Z isomers in the AAP monolayer as a function of time while the sample was kept in the dark. Initially the relative humidity was set to 5% (red squares), then changed to 28 % (black diamonds) and then changed back to 5 % (black circles).*

We have to point out that the apparent switching kinetics presented in Figure 5 are dominated by external factors such as the photon flux to the surface which can be used to accelerate or slow down the E/Z photoisomerization. This is consistent with earlier works of $E{\rightarrow}Z$ switching of azobenzene thiols on a gold surface by Krekiehn et al.[10] which do show an even more complicated behavior. This was caused by the short thermal lifetime of the Z state which also drastically affected the photostationary state for the classical azo derivatives used by these authors.

For our AAP photoswitches, the photostationary states are expected to be typically >90 % and exceptionally long thermal life times are expected as well which have been both reported before.[15,63] However, the stability of the Z configuration dissolved in chloroform was relatively poor and the molecules returned from the Z into the E state within minutes (Figure 2b), while in methanol the Z configuration was actually stable for many hours. Consequently, it is *a priori* not clear if the lifetime of the Z configuration in the monolayer is long enough to neglect thermal relaxation of the Z configuration. This calls for additional SFG experiments to reveal the stability of the Z form within the monolayer of surface-adsorbed AAP molecules. In order to gain information on the Z stability, we have done additional experiments in air of different relative humidity and report on the changes during transition from the Z to the E state under dark conditions (Figure 5c). Obviously, the effect of relative humidity is drastic as only a fraction of the molecules was able to thermally relax to the E state when the humidity was 28 % while at 5 % relative humidity almost all molecules returned to the E state. This can be concluded from a close comparison of the green irradiated sample with the thermalized sample (no light irradiation) in Figure 3a, where the SFG intensity of the thermalized sample is overall lower than the intensity of the green irradiated sample. This indicates that not all molecules have returned to the E state when the sample was kept in the dark.

For quantification of the thermal stability, we have again assumed first-order kinetics and fitted the results in Figure 5c using eqn. (16). The thermal lifetime that we have obtained from this analysis was 244 min for both conditions at 28 and 5 % relative humidity, which is an order of magnitude longer than the effective switching times when the samples where irradiated with UV light. Consequently, we can safely assume for the *butyl*-AAP-C$_{18}$ phosphonic acid monolayers in our study that thermal relaxation can be neglected on the time scale where the light-triggered changes occur. Thus, we conclude that the

intrinsic $E{\rightarrow}Z$ switching kinetics of the monolayer is by a factor of ≈ 91 faster (eqn. (18)) compared to the $Z{\rightarrow}E$ switching. We propose that the slower $Z{\rightarrow}E$ kinetics are likely due to a self-assembly process that requires more time to densely pack the molecules in their E configuration. Since the experiments were conducted in the presence of water, where the vapor phase had a relative humidity of <8 %, the interaction of water with the AAP monolayer has to be taken into account as well. This is corroborated by the study of Moldt et al.[9], who have shown for azobenzene monolayers that the switching kinetics can be severely affected by the presence of water and, where, the authors have proposed a stabilization of Z configuration through interaction with water. We believe that H_2O likely interacts with the exposed polar azo groups of the monolayer when the AAP moieties are in their Z state. From this discussion, we conclude that water needs to be considered as a relevant factor which can influence the switching kinetics and we will come back to this question when discussing the wetting dynamics in detail below.

Wetting dynamics of photo-switchable butyl-AAP-C$_{18}$ phosphonic acid monolayers

In Figure 6 we present the dynamic contact angle that was determined from a sessile drop of water in contact with a *butyl*-AAP-C$_{18}$ phosphonic acid monolayer at the α-Al$_2$O$_3$(0001) surface. Modification of the hydrophilic α-Al$_2$O$_3$(0001) surface with the AAP monolayer causes the contact angle Θ to increase to >83°, when the AAP moieties in the monolayer were in their E configuration which was prepared by prolonged exposure to green light. For the contact angle experiments, the samples were irradiated *in situ* with either 520 nm green or 365 nm UV light and the change of the light source was also performed *in situ* within <1 s, while the dynamic changes in Θ were continuously monitored. After initially depositing a drop of water on the surface, Θ already decreased with a certain rate which we attribute to a small degree of relaxation or adaptation of the monolayer when it is brought in contact with bulk water at the solid-liquid interface. Although the relative humidity of the vapor phase was with >90 % relatively high, also slow evaporation of the drop could additionally contribute to the changes on rather long time scales. The changes in contact angle are, however, much more pronounced and on a faster time scale when the light irradiation was switched from green to UV light which caused the $E{\rightarrow}Z$ photo-isomerization of the *butyl*-AAP-C$_{18}$ phosphonic acid monolayer. Here a sharper decrease in contact angle up to $|\Delta\Theta|{\sim}10°$ can be observed when the drop was brought in contact with the monolayer for the first time and then irradiated with UV light to initiate the E to Z switching of the monolayer.

Dewetting experiments where we irradiated the samples with green light to forcefully switch the monolayer back from the Z to the E state were unsuccessful. In fact, as long as the water drop was in contact with the monolayer, the contact angle that was established after $E{\rightarrow}Z$ switching could not be reversed to its initial higher value. However, we also observed reversible changes in contact angle, when the drop was first withdrawn from the surface, the monolayer exposed again to the vapor phase while it was continuously irradiated with green light. In that case, subsequent wetting of the identical surface area resulted in a reversible change by $|\Delta\Theta| \sim 6°$ (see Figure 6b). From this observation, we conclude that the monolayer can maintain its switching ability after wetting with water, but the energy barrier for $Z{\rightarrow}E$ switching is much higher when the monolayer is immersed in water. As a consequence the Z state remains 'frozen' and unable to change back into the E state when the light irradiation changes.
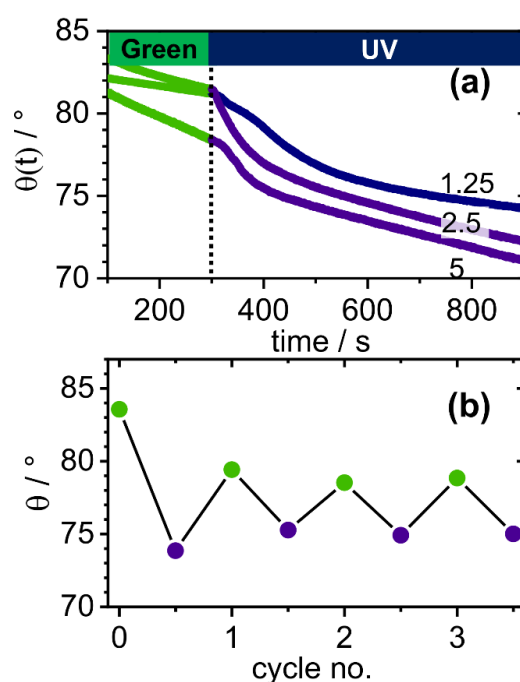
Figure 6. *(a) Dynamic changes in the contact angle for monolayers butyl-AAP-C_{18} phosphonic acids on α-$Al_2O_3(0001)$ as a function of time. For that a water drop with a volume of 10 µL was deposited on the surface under green light irradiation and after 300 s the irradiation was changed from green to UV light to induce the $E{\rightarrow}Z$ configurational change. This was done with fluence of 1.25, 2.5 and 5 mW/cm². (b) Shows the reversibility in switching of the static contact angle when the drop was removed from the surface, while the irradiation was changed and wetted again. For that the identical surface area was taken.*

This is consistent with our results from SFG spectroscopy of the monolayer in different relative humidity as well as with the work by Moldt et al.[9]. Although in the latter work, the authors have not studied the wetting dynamics of their azobenzene monolayers, but reported on the stabilization of the *Z* configuration in the presence of water from the vapor phase which resulted in different photostationary states and switching kinetics. In order to model the results with one of the two models presented in the Materials and Methods section we need to disentangle the effects of the slow relaxation of the layer and possibly also from the evaporation of the drop as well as from the light induced effects on the dynamic contact angle. Clearly any data analysis with the models for dynamic wetting is impaired by the slow process. For that reason, we have subtracted the almost linear contribution from our data (see Figure 6a at long times) and concentrate on the light triggered changes in more detail below. The corrected values are shown in Figures 7a and 7b where we plot $\cos\Theta(t)$ for the different fluence of the UV light as well as for two different droplet sizes which has allowed us to change the wetting dynamic within limits.

A close inspection of Figures 7a,b already reveals that the time scales of wetting dynamics are largely different from what one expects if the wettability changes with UV light would simply follow the molecular changes e.g. at the solid-vapor interface (1 to 15 s, Table 1). We point out that the dependence on the UV fluence as seen for the switching of the monolayer without direct contact with liquid water, is still present in the dynamic wetting experiment and is, consequently, indicative for the time needed to switch the substrate. Clearly, the switching kinetics of the photoswitchable substrate are of relevance to the dynamic contact angle. For a better understanding of the mutual interplay of switching kinetics and the resulting wetting dynamics we now resort to simulation and theoretical modelling.

Modelling the wetting dynamics with coupled substrate and drop dynamics

To capture the combined effects of the drop and substrate dynamic we have performed additional simulations using a Lennard Jones system (Materials and Methods) with a setup in close analogy to the experimental situation. In a first step we determined the values of ε_s where the contact angles have approximately the values as observed in the experiments of ~84° when the molecules in the layer are in their *E* configuration and ~73° when the molecules are in the *Z* state. From that we determine $\varepsilon_{s,E} = 0.3411$ and $\varepsilon_{s,Z} = 0.3816$ for *E* and *Z* states, respectively. In a further step we

equilibrated a droplet on a surface with the interaction parameter $\varepsilon_{s,E}$ and switched it instantaneously to $\varepsilon_{s,Z}$. Thus, we can extract the time dependent contact angle of this process and fit an exponential curve to the obtained values, yielding the relaxation time τ or the corresponding relaxation rate k.

From the SFG experiments (see above), we can conclude that the wettability of the surface does not change instantaneously and we, therefore, assumed that the parameter ε_s increases exponentially from $\varepsilon_{s,E}$ to $\varepsilon_{s,Z}$. with the relaxation time τ_e or, analogously, the switching rate $k_e = \frac{1}{\tau_e}$. In practice, we have updated the energy ε_s in sufficiently small time steps. To explore the interplay of substrate and wetting dynamics, we have also used different switching rates. Using the definition $r = \frac{k}{k_e}$ this can be expressed via different values of r. Note that a ratio of $r = 0$ means instantaneous switching.

The change of the contact angle with time for different values of r can be seen in Figure 7c, where we show the results for r-values between 0 and 16. If the substrate is switched infinitely slow, the droplet is fully equilibrated to the newly established wettability of the surface that is connected to the molecular changes in the substrate surface. In Figure 7d the time dependent contact angle of a switching process is plotted against the contact angle which the droplet would have if it was fully equilibrated to the instantaneous wettability at each time step. For $r \leq 1$ significant non-equilibrium effects are visible, i.e. the droplet dynamics are too slow to follow the switching of the substrate. These data can be taken to elucidate the relevance of the analytically solvable model that we have described in the Materials and Methods section and which boils down to eqn. (14). The model predictions are also plotted in Figure 7c and Figure 7d. Since the value of k is fixed from the simulation with infinitely fast switching, no adjustable parameters are involved. The very good agreement shows that despite its simplicity, the model captures the key aspects of the interplay of substrate and droplet dynamics. Having established that model, connecting the intrinsic characteristic time e.g. that of the AAP monolayer which modulates the wettability of the solid surface with the relaxation time of the drop, we can now apply this model to the experimental data in Figures 7a and 7b. Following the results for the switching of the monolayer we assume that its characteristic inverse switching time is proportional to the UV fluence. Specifically, for the experimentally chosen fluences (1.25, 2.5, 5 and 7 mW/cm²) we assume inverse switching times with ratios 1:2:4:5.
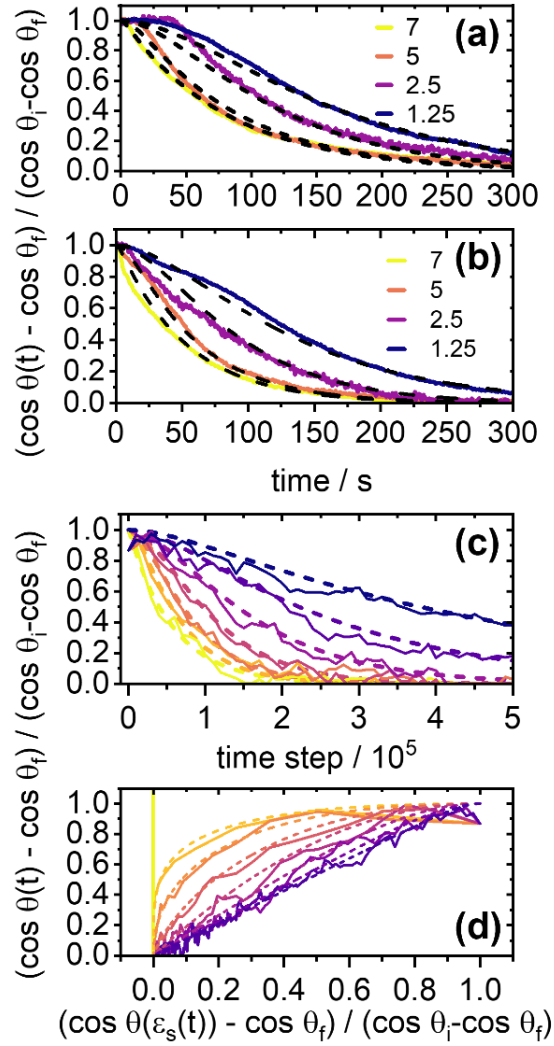
Figure 7. *(a) and (b) show the experimental results from a dynamic wetting experiment during E→Z switching with different fluence of the UV light in units of mW/cm² and for a drop volume of 20 and 10 µL, respectively. (c) Contact angles versus time step for different k/k_e ratios with 0 (infinitely fast switching of the substrate), 0.25, 0.5, 1, 2, 4, and 8 which are color coded from yellow to dark blue, respectively. In addition, we present the corresponding fits of the model function. The solid lines indicate the values from the simulations, while the dashed lines show the results of the model according to eqn. (14). The simulations have been performed for constant k and varying k_e.(d) Time dependent contact angle versus the equilibrium contact angle at the instantaneous wettability, using the same k/k_e values as in (c). The solid lines mark the values of the simulations, while the dashed lines the results of the model.*

Furthermore, we assume that these switching times do not depend on the volume of the droplet, i.e. are the same for the data presented in Figures 7a and 7b. Then we performed a global fit, based on eqn. (14) with three adjustable parameters for the whole set of data in these curves. These parameters are the inverse switching time k_e at the lowest UV fluence and the droplet relaxation rate k for each droplet volume (20 and 10 μL, respectively). The results of our fitting procedures are shown in Figure 7a,b where we find very good agreement with the experimental results. The characteristic times for the apparent dynamics of the substrate upon irradiation with UV light are summarized in Table 1, where they can be compared by the effective time constants of the non-wetted layer in the vapor phase. Note that in particular the plateau-like shape and small curvature at early times is inconsistent with the simple exponential relaxation model. This model assumes instantaneous equilibration of the drop to the new interface energies caused by *E* to *Z* switching. This is different in the analytical model (eqn. (14)) which is, in fact, capable of describing this peculiar feature of the dynamic contact angle. The characteristic times that we obtained for the drop dynamics are 80 and 52 s for a drop volume *V* of 20 and 10 μL, respectively. They are by factor of 1.55 different. According to earlier works[64] the characteristic time of the drop dynamic is suggested to scale with $\sqrt{V}$. The factor 1.55 that we gain from comparing the times for 20 and 10 μL is, thus, within expectation ($\sqrt{2}$). Furthermore, the assumption that the droplet relaxation does not depend on droplet size, seems to be fulfilled to a very good approximation. It is thus possible just from fitting the experimental data for the larger droplet to fully predict the outcome for the experiments with the smaller droplet. For low fluence the value of r as introduced above, is below or close to unity (in particular for the smaller droplet). Thus, we indeed have the situation that the droplet can no longer follow the switching process via its equilibrium shape.

From Table 1 one can observe that the difference between the characteristic times of the monolayer and for the dynamic contact angle is substantial and amounts to approximately a factor of 6. Thus, the presence of a water droplet slows down the relaxation process from the *E* to the *Z* configuration. In fact, the apparent differences in characteristic times is likely associated to friction caused by water molecules as suggested earlier by Johansson et al.[65] for wetting of silica surfaces. However, the approximately linear relation between UV fluence and switching time, as observed in pure monolayers, is still valid as seen from the high quality of the fit. This indicates that the mechanisms of the molecular switching of

the AAP monolayer remains similar. As an additional effect, hydrogen bonds between water and the exposed azo groups could be formed which do also keep the AAP layer locked in its *Z* configuration and increase the thermal stability of the *Z* state as discussed above.

Table 1 *Characteristic times for switching of the contact angle (CA) and the nonwetted monolayer in the vapor phase for different fluence of UV and green light irradiation. τ and τ_e correspond to the drop and substrate dynamic during wetting, respectively. $\tau_{E \to Z}$ and $\tau_{Z \to E}$ are the characteristic switching times of the monolayer in the absence of a wetting liquid.*

Fluence	CA 10 μL	CA 20 μL	CA	Monolayer	
mWcm^{-2}	τ / s	τ / s	τ_e / s	$\tau_{E \to Z}$ / s	$\tau_{Z \to E}$ / s
1.25	52	80	87	15	167
2.5	52	80	43	8	237
5	52	80	22	4	170
7	52	80	17	(1)^a	-

^{a} *Note that this value is based only on two data points due to the limited time resolution in the experiment (see Figure 6b).*

SUMMARY AND CONCLUSIONS

In this work we combine experiments and simulations in order to address both the molecular changes of a photoswitchable monolayer during *E*/*Z* photo-isomerization as well as the wetting dynamics that are caused by *E*→*Z* configurational changes of the monolayer while it is in contact with a drop of water. For that we have synthesized arylazopyrazole phosphonic acid molecules (*butyl*-AAP-C$_{18}$PA) and deposited these molecules on α-Al$_2$O$_3$(0001) single crystals. Using the Langmuir-Blodgett technique, we have adjusted the surface density of *butyl*-AAP-C$_{18}$ phosphonic acids to 6.7±0.5 molecules/nm^2. This surface density facilitates large changes in molecular structure that we have interrogated by applying time-dependent vibrational SFG spectroscopy, while the interaction of water with the AAP layers was additionally investigated with MD simulations. They show that the density used in our experiments is high enough to avoid penetration of water into the layer and, thus, to prevent an unwanted complexity during wetting of the layers. *E*→*Z* switching of the monolayers is relatively fast in the vapor phase, where the characteristic time of the switching process is linearly dependent on fluence of the UV light used to trigger the process. Characteristic times for *E*→*Z* switching range between 1 and 15 s, whereas

$Z{\rightarrow}E$ switching is with ~160 s considerably slower. This difference is attributed to a slow self-organization process for the Z to the E transition. Further, we demonstrate that water can stabilize the Z configuration and even lock the molecules in this state. This has far reaching consequences for the wetting behavior, because the layer cannot be switched back to the E configuration while it is in contact with water. Additional experiments and simulations were performed in order to decouple the effects of drop and substrate dynamics on the dynamic contact angle. We show that the characteristic times of both processes need to be considered in a wetting experiments. Based on a minimalistic model, verified for a simulation setup based on Lennard-Jones particles on a substrate, we could indeed disentangle both processes in a quantitative manner. It turns out that the characteristic times for the drop and the substrate dynamics are very similar and within 50 to 150 s, where we show that the dynamics can be adjusted in a way that the drop dynamic is either directly following the wettability changes of the substrate or that the drop is too slow to follow. In addition, the wetting transition during $E{\rightarrow}Z$ photoisomerization is on a different time scale as compared to the monolayer in the vapor phase. This is attributed to additional friction that is likely caused by water molecules forming hydrogen bond to the exposed azo groups, which do also contribute to the stabilization of the Z configuration.

ASSOCIATED CONTENT

Supporting Information

The Supporting Information is available free of charge at

In the SI we present information on the synthesis procedures and the Langmuir-Blodgett disposition of the arylazopyrazole monolayers. Further analysis of SFG spectra, band assignment as well as details on the fitting parameters used to model the SFG spectra.

AUTHOR INFORMATION

Corresponding author

*e-mail: braunschweig@uni-muenster.de

ORCID

Björn Braunschweig: 0000-0002-6539-1693

Andreas Heuer: 0000-0003-2592-0287

Natalia García Rey: 0000-0002-9175-3416

Leon Topp: 0000-0003-4568-4357

References

(1) Feng, L.; Li, S.; Li, Y.; Li, H.; Zhang, L.; Zhai, J.; Song, Y.; Liu, B.; Jiang, L.; Zhu, D. Super-Hydrophobic Surfaces: From Natural to Artificial. *Adv. Mater.* **2002**, *14* (24), 1857–1860.

(2) Li, J.; Ha, N. S.; Liu, T. '.; van Dam, R. M.; 'CJ' Kim, C.-J. Ionic-Surfactant-Mediated Electro-Dewetting for Digital Microfluidics. *Nature* **2019**, *572* (7770), 507–510.

(3) Russew, M.-M.; Hecht, S. Photoswitches: From Molecules to Materials. *Adv. Mater.* **2010**, *22* (31), 3348–3360.

(4) Butt, H.-J.; Berger, R.; Steffen, W.; Vollmer, D.; Weber, S. A. L. Adaptive Wetting—Adaptation in Wetting. *Langmuir* **2018**, *34* (38), 11292–11304.

(5) Tadmor, R. Open Problems in Wetting Phenomena: Pinning Retention Forces. *Langmuir* **2021**, *37* (21), 6357–6372.

(6) Meltzer, C.; Yu, H.; Peukert, W.; Braunschweig, B. Molecular Structure of Octadecylphosphonic Acids During Their Self-Assembly on α-Al$_2$O$_3$(0001). *Phys. Chem. Chem. Phys.* **2018**, *20* (29), 19382–19389.

(7) Katsonis, N.; Kudernac, T.; Walko, M.; van der Molen, S. J.; van Wees, B. J.; Feringa, B. L. Reversible Conductance Switching of Single Diarylethenes on a Gold Surface. *Adv. Mater.* **2006**, *18* (11), 1397–1400.

(8) Kortekaas, L.; Ivashenko, O.; van Herpt, J. T.; Browne, W. R. A Remarkable Multitasking Double Spiropyran: Bidirectional Visible-Light Switching of Polymer-Coated Surfaces with Dual Redox and Proton Gating. *J. Am. Chem. Soc.* **2016**, *138* (4), 1301–1312.

(9) Moldt, T.; Przyrembel, D.; Schulze, M.; Bronsch, W.; Boie, L.; Brete, D.; Gahl, C.; Klajn, R.; Tegeder, P.; Weinelt, M. Differing Isomerization Kinetics of Azobenzene-Functionalized Self-Assembled Monolayers in Ambient Air and in Vacuum. *Langmuir* **2016**, *32* (42), 10795–10801.

(10) Krekiehn, N. R.; Müller, M.; Jung, U.; Ulrich, S.; Herges, R.; Magnussen, O. M. UV/Vis Spectroscopy Studies of the Photoisomerization Kinetics in Self-Assembled Azobenzene-Containing Adlayers. *Langmuir* **2015**, *31* (30), 8362–8370.

(11) Umlandt, M.; Feldmann, D.; Schneck, E.; Santer, S. A.; Bekir, M. Adsorption of Photoresponsive Surfactants at Solid–Liquid Interfaces. *Langmuir* **2020**, *36* (46), 14009–14018.

(12) Valley, D. T.; Onstott, M.; Malyk, S.; Benderskii, A. V. Sself-Assembled Monolayers of Azobenzene and Alkane Thiols. *Langmuir* **2013**, *29* (37), 11623–11631.

(13) Weston, C. E.; Richardson, R. D.; Haycock, P. R.; White, A. J. P.; Fuchter, M. J. Arylazopyrazoles: Azoheteroarene Photoswitches Offering Quantitative Isomerization and Long Thermal Half-Lives. *J. Am. Chem. Soc.* **2014**, *136* (34), 11878–11881.

(14) Nguyen, D. T.; Freitag, M.; Gutheil, C.; Sotthewes, K.; Tyler, B. J.; Böckmann, M.; Das, M.; Schlüter, F.; Doltsinis, N. L.; Arlinghaus, H. F.; Ravoo, B. J.; Glorius, F. An Arylazopyrazole-Based N-Heterocyclic Carbene as a Photoswitch on Gold Surfaces: Light-Switchable Wettability, Work Function, and Conductance. *Ang. Chem. Int. Ed.* **2020**, *59* (32), 13651–13656.

(15) Honnigfort, C.; Campbell, R. A.; Droste, J.; Gutfreund, P.; Hansen, M. R.; Ravoo, B. J.; Braunschweig, B. Unexpected Monolayer-to-Bilayer Transition of Arylazopyrazole Surfactants Facilitates Superior Photo-Control of Fluid Interfaces and Colloids. *Chem. Sci.* **2020**, *11* (8), 2085–2092.

(16) Schnurbus, M.; Stricker, L.; Ravoo, B. J.; Braunschweig, B. Smart Air-Water Interfaces with Arylazopyrazole Surfactants and Their Role in Photoresponsive Aqueous Foam. *Langmuir* **2018**, *34* (21), 6028–6035.

(17) Seshadri, S.; Bailey, S. J.; Zhao, L.; Fisher, J.; Sroda, M.; Chiu, M.; Stricker, F.; Valentine, M. T.; Read de Alaniz, J.; Helgeson, M. E. Influence of Polarity Change and Photophysical Effects on Photosurfactant-Driven Wetting. *Langmuir* **2021**, *37*, 9939–9951.

(18) Schnurbus, M.; Campbell, R. A.; Droste, J.; Honnigfort, C.; Glikman, D.; Gutfreund, P.; Hansen, M. R.; Braunschweig, B. Photo-Switchable Surfactants for Responsive Air–Water Interfaces: Azo versus Arylazopyrazole Amphiphiles. *J. Phys. Chem. B* **2020**, *124* (31), 6913–6923.

(19) Moldt, T.; Brete, D.; Przyrembel, D.; Das, S.; Goldman, J. R.; Kundu, P. K.; Gahl, C.; Klajn, R.; Weinelt, M. Tailoring the Properties of Surface-Immobilized Azobenzenes by Monolayer Dilution and Surface Curvature. *Langmuir* **2015**, *31* (3), 1048–1057.

(20) Yan, H.; Qiu, Y.; Wang, J.; Jiang, Q.; Wang, H.; Liao, Y.; Xie, X. Wholly Visible-Light-Responsive Host-Guest Supramolecular Gels Based on Methoxy Azobenzene and β-Cyclodextrin Dimers. *Langmuir* **2020**, *36* (26), 7408–7417.

(21) Chevallier, E.; Mamane, A.; Stone, H. A.; Tribet, C.; Lequeux, F.; Monteux, C. Pumping-Out Photo-Surfactants from an Air–Water Interface Using Light. *Soft Matter* **2011**, *7* (17), 7866.

(22) Fu, W.; Pi, Y.; Gao, M.; Wang, W.; Li, C.; Tan, R.; Yin, D. Light-Controlled Cooperative Catalysis of Asymmetric Sulfoxidation Based on Azobnzene-Bridged Chiral Salen Ti(IV)-Catalysts. *Chem. Commun.* **2020**, *56* (44), 5993–5996.

(23) Nagai, Y.; Ishiba, K.; Yamamoto, R.; Yamada, T.; Morikawa, M.-A.; Kimizuka, N. Light-Triggered, Non-Centrosymmetric Self-Assembly of Aqueous Arylazopyrazoles at the Air-Water Interface and Switching of Second-Harmonic Generation. *Ang. Chem. Int. Ed.* **2021**, *60* (12), 6333–6338.

(24) Simke, J.; Böckermann, T.; Bergander, K.; Klabunde, S.; Hansen, M. R.; Ravoo, B. J. Photoresponsive Host-Guest Chemistry and Relaxation Time of Fluorinated Cyclodextrin and Arylazopyrazole-Functionalized DOTA Metal Complexes. *Org. Bioorg. Chem.* **2021**, *19* (10), 2186–2191.

(25) Kwon, G.; Panchanathan, D.; Mahmoudi, S. R.; Gondal, M. A.; McKinley, G. H.; Varanasi, K. K. Visible light Guided Manipulation of Liquid Wettability on Photoresponsive Surfaces. *Nat. Commun.* **2017**, *8*, 14968 EP -.

(26) Groten, J.; Bunte, C.; Rühe, J. Light-Induced Switching of Surfaces at Wetting Transitions through Photoisomerization of Polymer Monolayers. *Langmuir* **2012**, *28* (42), 15038–15046.

(27) Ariga, K. Don't Forget Langmuir–Blodgett Films 2020: Interfacial Nanoarchitectonics with Molecules, Materials, and Living Objects. *Langmuir* **2020**, *36* (26), 7158–7180.

(28) Lambert, A. G.; Davies, P. B.; Neivandt, D. J. Implementing the Theory of Sum Frequency Generation Vibrational Spectroscopy: A Tutorial Review. *Appl. Spectrosc. Rev.* **2005**, *40* (2), 103–145.

(29) Shen, Y. R. Basic Theory of Surface Sum-Frequency Generation. *J. Phys. Chem. C* **2012**, *116* (29), 15505–15509.

(30) Shultz, M. J.; Schnitzer, C.; Simonelli, D.; Baldelli, S. Sum Frequency Generation Spectroscopy of The Aqueous Interface: Ionic and Soluble Molecular Solutions. *Int. Rev. Phys. Chem.* **2000**, *19* (1), 123–153.

(31) Zhang, C. Sum Frequency Generation Vibrational Spectroscopy for Characterization of Buried Polymer Interfaces. *Appl. Spectrosc.* **2017**, *71* (8), 1717–1749.

(32) Wang, H.-F.; Velarde, L.; Gan, W.; Fu, L. Quantitative Sum-Frequency Generation Vibrational Spectroscopy of Molecular Surfaces and Interfaces: Lineshape, Polarization, and Orientation. *Annu. Rev. Phys. Chem.* **2015**, *66* (1), 189–216.

(33) Richmond, G. L. Molecular Bonding and Interactions at Aqueous Surfaces as Probed by Vibrational Sum Frequency Spectroscopy. *Chem. Rev.* **2002**, *102* (8), 2693–2724.

(34) García Rey, N.; Weißenborn, E.; Schulze-Zachau, F.; Gochev, G.; Braunschweig, B. Quantifying Double-Layer Potentials at Liquid-Gas Interfaces from Vibrational Sum-Frequency Generation. *J. Phys. Chem. C* **2019**, *123* (2), 1279–1286.

(35) Berendsen, H. J. C.; van der Spoel, D.; van Drunen, R. GROMACS: A Message-Passing Parallel Molecular Dynamics Implementation. *Comp. Phys. Commun.* **1995**, *91* (1), 43–56.

(36) Wang, J.; Wolf, R. M.; Caldwell, J. W.; Kollman, P. A.; Case, D. A. Development and Testing of a General Amber Force Field. *J. Comp. Chem.* **2004**, *25* (9), 1157–1174.

(37) Wang, J.; Wang, W.; Kollman, P. A.; Case, D. A. Automatic Atom Type and Bond Type Perception in Molecular Mechanical Calculations. *J. Mol. Grap. Mod.* **2006**, *25* (2), 247–260.

(38) Ditchfield, R.; Hehre, W. J.; Pople, J. A. Self-Consistent Molecular-Orbital Methods. IX. An Extended Gaussian-Type Basis for Molecular-Orbital Studies of Organic Molecules. *J. Chem. Phys.* **1971**, *54* (2), 724–728.

(39) Hehre, W. J.; Ditchfield, R.; Pople, J. A. Self—Consistent Molecular Orbital Methods. XII. Further Extensions of Gaussian—Type Basis Sets for Use in Molecular Orbital Studies of Organic Molecules. *J. Chem. Phys.* **1972**, *56* (5), 2257–2261.

(40) Hariharan, P. C.; Pople, J. A. The Influence of Polarization Functions on Molecular Orbital Hydrogenation Energies. *Theo. Chim. acta* **1973**, *28* (3), 213–222.

(41) Francl, M. M.; Pietro, W. J.; Hehre, W. J.; Binkley, J. S.; Gordon, M. S.; DeFrees, D. J.; Pople, J. A. Self-Consistent Molecular Orbital Methods. XXIII. A Polarization-Type Basis Set for Second-Row Elements. *J. Chem. Phys.* **1982**, *77* (7), 3654–3665.

(42) Essmann, U.; Perera, L.; Berkowitz, M. L.; Darden, T.; Lee, H.; Pedersen, L. G. A Smooth Particle Mesh Ewald Method. *J. Chem. Phys.* **1995**, *103* (19), 8577–8593.

(43) Yeh, I.-C.; Berkowitz, M. L. Ewald Summation for Systems with Slab Geometry. *J. Chem. Phys.* **1999**, *111* (7), 3155–3162.

(44) Bussi, G.; Donadio, D.; Parrinello, M. Canonical Sampling Through Velocity Rescaling. *J. Chem. Phys.* **2007**, *126* (1), 14101.

(45) Hess, B. P-LINCS: A Parallel Linear Constraint Solver for Molecular Simulation. *J. Chem. Theo. Comp.* **2008**, *4* (1), 116–122.

(46) Jorgensen, W. L.; Chandrasekhar, J.; Madura, J. D.; Impey, R. W.; Klein, M. L. Comparison of Simple Potential Functions for Simulating Liquid Water. *J. Chem. Phys.* **1983**, *79* (2), 926–935.

(47) Humphrey, W.; Dalke, A.; Schulten, K. VMD: Visual Molecular Dynamics. *J. Mol. Grap.* **1996**, *14* (1), 33–38.

(48) Anderson, J. A.; Glaser, J.; Glotzer, S. C. HOOMD-Blue: A Python Package for High-Performance Molecular Dynamics and Hard Particle Monte Carlo Simulations. *Comp. Mat. Sci.* **2020**, *173*, 109363.

(49) Hoogerbrugge, P. J.; J. M. V. A Koelman. Simulating Microscopic Hydrodynamic Phenomena with Dissipative Particle Dynamics. *Europhysics Letters (EPL)* **1992**, *19* (3), 155–160.

(50) Phillips, C. L.; Anderson, J. A.; Glotzer, S. C. Pseudo-Random Number Generation for Brownian Dynamics and Dissipative Particle Dynamics Simulations on GPU Devices. *J. Comp. Phys.* **2011**, *230* (19), 7191–7201.

(51) Blake, T. D.; Haynes, J. M. Kinetics of Liquid-Liquid Displacement. *J. Coll. Int. Sci.* **1969**, *30* (3), 421–423.

(52) Grawitter, J.; Stark, H. Steering Droplets on Substrates Using Moving Steps in Wettability. *Soft Matter* **2021**, *17* (9), 2454–2467.

(53) Ruijter, M. J. de; Coninck, J. de; Blake, T. D.; Clarke, A.; Rankin, A. Contact Angle Relaxation During the Spreading of Partially Wetting Drops. *Langmuir* **1997**, *13* (26), 7293–7298.

(54) Riaz, S.; Friedrichs, G. Vibrational Sum-Frequency Generation Study of Molecular Structure, Sterical Constraints and Nonlinear Optical Switching Contrast of Mixed Alkyl-Azobenzene Self-Assembled Monolayers. *Z. Phys. Chem.* **2020**, *234* (7-9), 1427–1452.

(55) Backus, E. H. G.; Kuiper, J. M.; Engberts, J. B. F. N.; Poolman, B.; Bonn, M. Reversible Optical Control of Monolayers on Water Through Photoswitchable Lipids. *J. Phys. Chem. B* **2011**, *115* (10), 2294–2302.

(56) Ward, R. N.; Duffy, D. C.; Davies, P. B.; Bain, C. D. Sum-Frequency Spectroscopy of Surfactants Adsorbed at a Flat Hydrophobic Surface. *J. Phys. Chem.* **1994**, *98* (34), 8536–8542.

(57) Tyrode, E.; Hedberg, J. A Comparative Study of the CD and CH Stretching Spectral Regions of Typical Surfactants Systems Using VSFS: Orientation Analysis of the Terminal CH_3 and CD_3 Groups. *J. Phys. Chem. C* **2012**, *116* (1), 1080–1091.

(58) Bell, G. R.; Bain, C. D.; Ward, R. N. Sum-Frequency Vibrational Spectroscopy of Soluble Surfactants at the Air/Water Interface. *Faraday Trans.* **1996**, *92* (4), 515.

(59) Gautam, K. S.; Schwab, A. D.; Dhinojwala, A.; Zhang, D.; Dougal, S. M.; Yeganeh, M. S. Molecular Structure of Polystyrene at Air/Polymer and Solid/Polymer Interfaces. *Phys. Rev. Lett.* **2000**, *85* (18), 3854–3857.

(60) Novak, M.; Jäger, C. M.; Rumpel, A.; Kropp, H.; Peukert, W.; Clark, T.; Halik, M. The Morphology of Integrated Self-Assembled Monolayers and Their Impact on Devices – A Computational and Experimental Approach. *Org. Electr.* **2010**, *11* (8), 1476–1482.

(61) Pathak, A.; Bora, A.; Braunschweig, B.; Meltzer, C.; Yan, H.; Lemmens, P.; Daum, W.; Schwartz, J.; Tornow, M. Nanocylindrical Confinement Imparts Highest Structural Order in Molecular Self-Assembly of Organophosphonates on Aluminum Oxide. *Nanoscale* **2017**, *9* (19), 6291–6295.

(62) Schleeger, M.; Nagata, Y.; Bonn, M. Quantifying Surfactant Alkyl Chain Orientation and Conformational Order from Sum Frequency Generation Spectra of CH Modes at the Surfactant-Water Interface. *J. Phys. Chem. Lett.* **2014**, *5* (21), 3737–3741.

(63) Stricker, L.; Fritz, E.-C.; Peterlechner, M.; Doltsinis, N. L.; Ravoo, B. J. Arylazopyrazoles as Light-Responsive Molecular Switches in Cyclodextrin-Based Supramolecular Systems. *J. Am. Chem. Soc.* **2016**, *138* (13), 4547–4554.

(64) Zhang, J.; Borg, M. K.; Reese, J. M. Multiscale Simulation of Dynamic Wetting. *Int. J. Heat Mass Transfer* **2017**, *115*, 886–896.

(65) Johansson, P.; Carlson, A.; Hess, B. Water–Substrate Physico-Chemistry in Wetting Dynamics. *J. Fluid Mech.* **2015**, *781*, 695–711.

TABLE of CONTENT GRAPHIC